Effects of jet in crossflow on flame acceleration and deflagration to detonation transition in methane-oxygen mixture

Han Peng[1], Yue Huang[1*], Ralf Deiterding[2], Zhenye Luan[1], Fei Xing[1], Yancheng You[1]

[1]School of Aerospace Engineering, Xiamen University, Xiamen, 361005, China
[2]Faculty of Engineering and the Environment, University of Southampton, Southampton SO17 1BJ, UK

Abstract: The fluidal jet turbulator has been a novel perturbation generator in the pulse-detonation engines research field for the past few years. In this paper, an experiment is performed to study the deflagration to detonation transition (DDT) process in a detonation chamber with a reactive transverse methane-oxygen mixture jet in crossflow (JICF). The jet injection arrangement is fundamentally investigated, including single jet and various double jets patterns. Corresponding two-dimensional direct numerical simulations with a multistep chemical kinetics mechanism are employed for analyzing details in the flow field, and the interaction between the vortex and flame temporal evolution is characterized. Both the experiments and simulations demonstrate that the JICF can distinctly accelerate flame propagation and shorten the DDT time and distance. The vortex stream induced by the jet distorts and wrinkles the flame front resulting in local flame acceleration. Moreover, the double jet patterns enhance flame acceleration more than the single jet injection because of the intrinsic counter-rotating vortex pairs and enhanced turbulence intensity.

Keywords: flame acceleration; deflagration to detonation transition; jet in crossflow; flame-vortex interactions; methane flame

1. Introduction

Pulsed-detonation engines (PDEs) have been proposed as an advanced and developing propulsion system with potential advantages including high thermodynamic efficiency and structural simplicity [1-3]. Although detonations have outstanding energetic advantages compared to conventional constant pressure combustion processes, a lot of challenges remain to be solved due to their unstable and complex characteristics. One of challenges for PDE research is the implementation of low energy ignition to initiate stable detonation waves within a short distance and time [4]. The detonation can be formed through the Deflagration-to-Detonation Transition (DDT) process. However, a detonation tube with smooth walls will be too long to accomplish the DDT process for engineering applications.

To shorten the DDT distance, various perturbation enhancement devices have been designed [5]. High-intensity turbulence generation is vital for flame acceleration. Traditionally, solid obstacles have been used to effectively shorten the DDT time and distance [6]. The presence of the obstacles leads to the formation of a laminar vortex ahead of the flame and induces turbulence within the reactant flow. In the initial stage, the flame acceleration is mainly due to flame wrinkling. The main reason for flame

wrinkling is the flame-vortex interaction, which is formed behind the obstacles [7]. The obstacles play another significant role to produce localized explosions. When the flame velocity reaches the local sound speed, a shock wave is formed ahead of the flame tip which compresses unburned gas. Then the detonations appear from hot spots created by shock reflections at corners between obstacles and the wall [8].

The goal of most previous studies on obstacles was to initiate a detonation at a shortest DDT length, but they did not consider practical engine cycle issues. In fact, the pressure losses have very important influence on PDE thrust performance in multi cycle PDE. A large blocking ratio increases the time of fresh mixture filling, limiting the operating frequency of PDE [9]. Large obstacles also act as thermal reservoirs, adding and subtracting heat at improper time in the PDE's cycle. Therefore, the design of turbulence enhancement devices for DDT processes needs to balance the acceleration gain and the total pressure loss.

The concept of jet obstacles has been proposed in conventional combustor recirculation zone design for ensuring combustion stability, where it leads to less total pressure loss compared to solid obstacles [10]. Inspired by this, the fluidic jet is applied as a substitute for a solid obstacle in the detonation chamber. Several relevant experiments were carried out to study the effect of fluidic jet on the DDT process. When the main flow consists of a stoichiometric hydrogen-air mixture and the jet composition is either premixed stoichiometric hydrogen-air or pure air, the results show that the jet plays the role of a virtual obstacle but suffers from substantially lower total pressure losses than a solid obstacle with similar blockage shape. But there is no discernable difference in DDT distances between the jet composition of air and reactive mixture [11-12]. Whereas in another study, the jet made by pure air deteriorates the local kerosene-air ratio and fuel distribution, which was observed experimentally and found to be disadvantageous for flame propagation. On the other hand, a jet made by a kerosene-air mixture can effectively accelerate the flame-propagation [13]. Apart from that, the experiments, methane-air flame acceleration in duct with JICF, demonstrate that the jet is more effective at transitioning the laminar flame to a fast-propagating turbulent flame than the solid object according to PIV and Schlieren imaging results [14]. This research about fluidic jet influence on the primary stages of the DDT process indicates that the jet induces increased turbulence through flow transport enhancement and entrainment mechanisms. The flow instabilities are strengthened with the jet stream, subsequently the velocity fluctuation and high turbulence intensities increase the reaction rates, leading to higher flame propagation speeds. At the next stage, the turbulent flame accelerates in the broken reaction regime during the jet-flame interaction, where detonation is expected to occur [15-16].

Although a lot of work has been conducted to study the effect of a single fluidic obstacle on flame acceleration and DDT progress, little attention was paid to the jet arrangement. The jets composed by inert gas or oxidizer evidently affected the local concentration and heterogeneity of the reactant, but utilizing the fuel-oxidant mixture jet poses risks in experimental safety. High resolution numerical simulations is a feasible way to get details about the flow field and flame evolution in the DDT process [17]. Two- and three-dimensional simulations with one step Arrhenius chemical model or detailed chemical mechanism both show that solid obstacles in a detonation chamber can induce vorticities and enhance the turbulent intensity downstream. The initial thermal diffusion and hydrodynamic instability play significant roles on flame acceleration. The solid obstacles reflect the precursor shock resulting in hot spots in the preheat region. The hot spots and the local concentration

gradient are considered as the main mechanism to trigger the transition to detonation [18-21]. However, the effect of a fluidal jet turbulator on the flame propagation in a DDT process has not been explored by numerical simulations yet.

In this paper, the effects of a reactive mixture JICF on the DDT process are investigated by both experiments and simulations. High speed photography was used to capture flame front position and velocity in the experiments. Detailed reactive flame-jet interactions were explored by numerical simulations. In addition, the discrepancies of the DDT process among various jet injection patterns are analyzed in this work, which aims to enhance the understanding of DDT with fluidic jets and contributes experimental data to identify mechanisms that can be used to optimize further the design of detonation combustors.

2. Experimental setup and numerical methods

2.1 Experimental setup

The test section was designed with a total viewable length of L = 800 mm and rectangle cross-section of W×H (width × height) = 6 mm×20 mm. The main structure is made of stainless steel. Acrylic glass is used on one side to enable high-speed photography. Its thickness is 5mm to balance the durability and transmittance. The experimental setup consists of the fuel and oxygen supply system, flow control system, the data acquisition system, ignition system, the test stands and the detonation channel (see Fig. 1). The mixtures in the detonation channel is ignited by spark plug with 50 mJ ignition energy, which is located at the center of the left end wall. The delay controller is composed of ARM-STM32F103CB development boards and an Ingenex-H3MB-052D solid-state relay. The signal is switched by the relay, whose active time and reset time are less than 1ms. The jet delay time is defined by the signal transmitting time interval between ignition and injection trigger as depicted in Fig. 2. The jet delay time of all the cases in this study is set to 0.4ms consistently. The solenoid valve (MAC 33A-AAB-RDFA-1BA) is used to control the jet injection and its energizing and de-energizing response time is 0.5ms and 0.2ms, respectively. Figure 3 displays the detailed arrangement of detonation channel and jet patterns. Initially, the tube is filled with a premixed stoichiometric CH4/O2 mixture from the premixed gas inlet, which is located at the middle of the tube and plays the role of exhaust during the evacuation stage. Then, the premixed gas inlet is closed by a ball valve. The tube initial static pressure is 0.06 MPa and the temperature is 293K before ignition. The right end of the tube is sealed by a polyethylene terephthalate thin film. Its thickness is 0.3mm and it will break if the pressure is more than 0.3Mpa. It not only ensures that the film is unbroken during the evacuation stage, but also ensures that the detonation can easily break the film and vent. The diameter of the jet holes is 1 mm. The jets are located at 90 mm and 180 mm away from the left wall with initial total pressure 0.2 MPa, stagnation temperature 293K and the same mixture concentration as the main flow. The injection patterns of the investigated cases are shown in Table 1. It is noted that the plugged small jet holes and measurement holes on the walls play a role as wall cavities (diameter 1mm, depth 5mm), which have an influence on the relatively small scale experiment. The maximum negative pressure of the vacuum pump is 10 kPa, which means that there is 10% air in the mixing chamber and test channel. Therefore, the mixture is not perfectly stoichiometric CH4/O2.

A FASTCAM MINI-AX200 high-speed camera is used to record the flame-flow characteristics with frequency 96000fps, where the resolution is set as 1024×48 pixel. The flame front spacing of two adjacent frames is measured, and the flame propagation velocity is obtained by dividing the corresponding time interval. The measurement error of this method is calculated through dividing the actual physics distance of the unit pixels in the spatial resolution by the exposure time of the image, which is about ±80m/s.

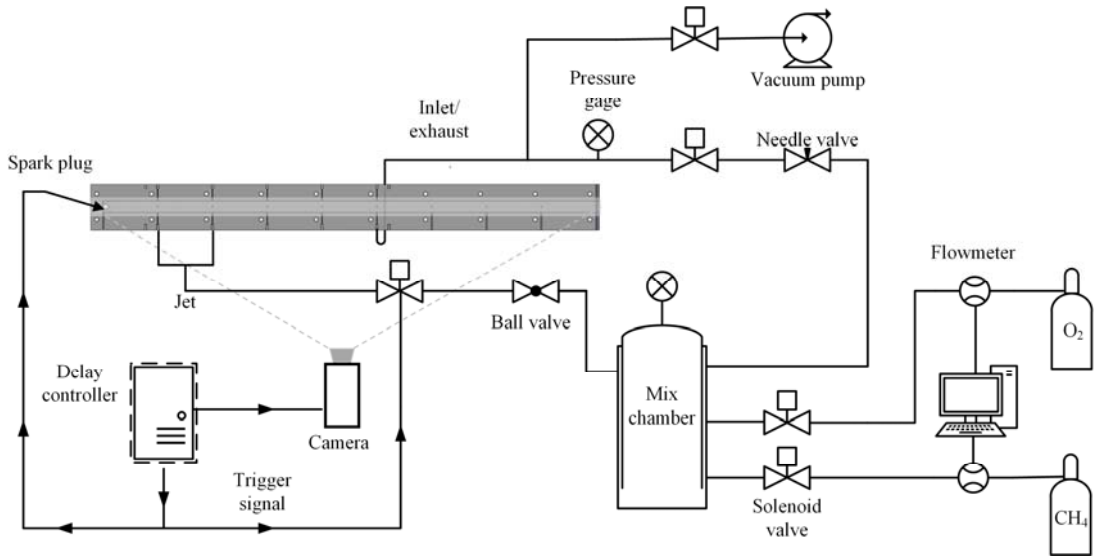

Fig. 1. Schematic of experimental setup.

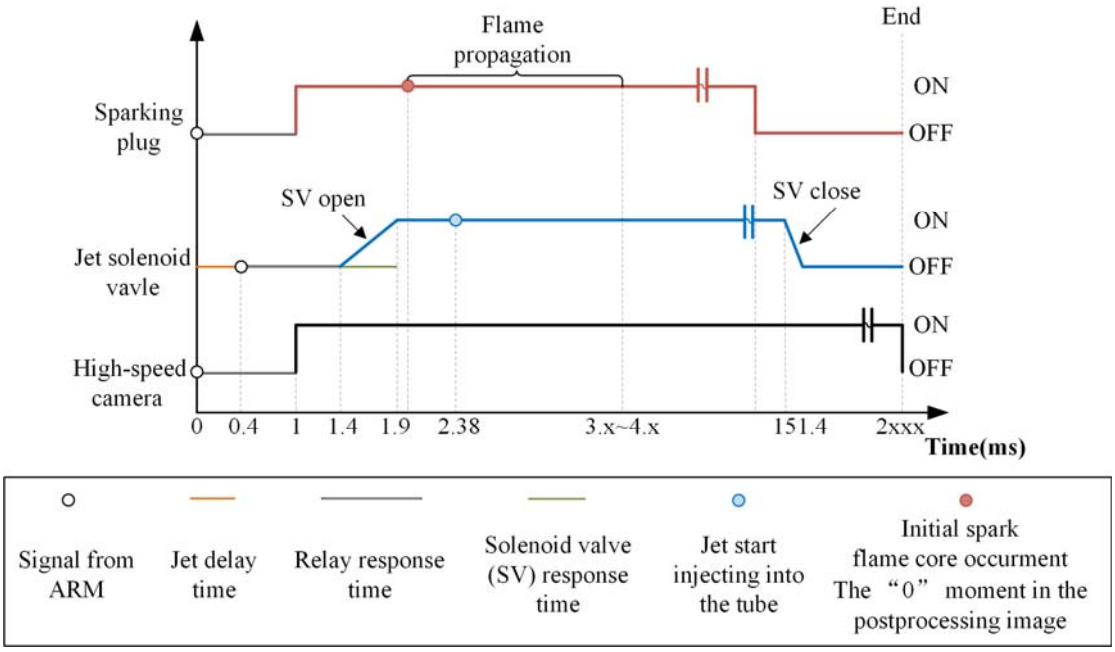

Fig. 2. Time sequence of the control signals

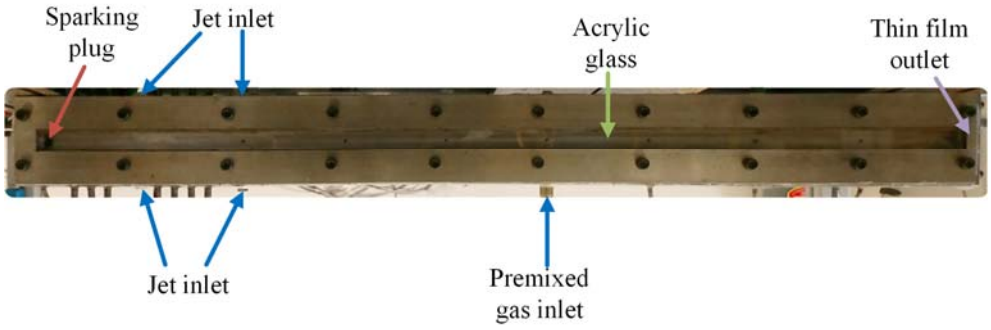

(a) Photograph of the experimental device

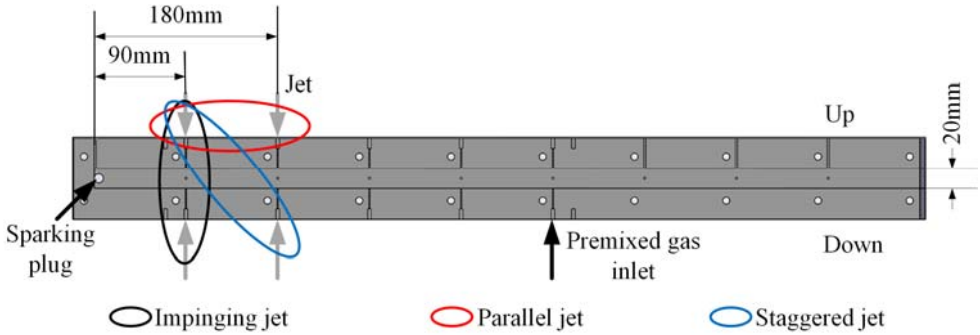

(b) Jet pattern schematic diagram

Fig. 3. Structure of detonation channel.

Table 1. Jet arrangements of the investigated cases.

Case number	Jet injection position	Injection pattern
1	None	—
2	90mm(down)	Single jet
3	180mm(down)	Single jet
4	90mm	Impinging jets
5	180mm	Impinging jets
6	90＆180mm(down)	Parallel jets
7	90mm(down)＆180mm(up)	Staggered jets

2.2 Numerical methods and calculation setup

The open-source program AMROC (Adaptive Mesh Refinement Object-oriented C++) [22] was adopted for the deflagration to detonation transition simulations. The high-speed combustion solver within AMROC has been validated for parallel numerical simulations of multi-dimensional detonation combustion in many studies [23-26].

The two-dimensional viscid unsteady reactive Navier-Stokes equations with the perfect gas equation of state are used as the governing equations for the simulations. A hybrid Roe-HLL [22] Riemann solver is utilized to construct inter-cell numerical upwind fluxes. The Minmod limiter with MUSCL reconstruction is applied to construct a second-order method in space. A conservative second-order accurate centred difference scheme is used for the diffusive term.

A second-order accurate Strang splitting method is adopted for the source term. Furthermore, a semi-implicit generalized Runge–Kutta method of fourth order (GRK4A) is utilized for the integration of the chemical kinetics [22]. A simplified chemical kinetic mechanism [27] for $CH_4/O_2/N_2$ was used to model the chemical reaction of the DDT process. The mechanism contains 14 species and 19 elementary reactions and it has been used to simulate detonation combustion successfully [28].

As shown in Fig. 4, the computational domain is a 2D rectangle channel with a length of 800 mm and a width of 20 mm, corresponding to the experiment. The channel is closed at the left end (x = 0) and open to the atmosphere at the opposite end (x = L). The bottom and top walls, as well as the left one, are adiabatic no-slip walls, while the right boundary is set as an open end. A semicircle region of hot burned material with temperature T = 2500 K is initialized to ignite the flame weakly. The circle center is positioned in the middle of the channel left wall and its radius is 4 mm. The temperature outside the circle is set to 293 K. The pressure in the whole fluid domain is set to 0.06 MPa. Unlike the experimental condition, the initial mixture in the simulations is diluted with 25% nitrogen in order to refer to several test results. The latter mimics estimated air evacuation impurities present in the experiments, cf. Section 3.1.2, but also aims at reducing the reactivity slightly in order to allow comparison of the two-dimensional simulations with experiments that are inherently three-dimensional in nature. The width of the jet is 1 mm, the initial jet total pressure is 0.2 MPa and the stagnation temperature is 293 K. The injection patterns are completely consistent with the jet arrangements in the experiment as shown in Table 1. The computational base cell size is set to 0.5 mm × 0.5 mm and refined to up to 0.0625 mm × 0.0625 mm adaptively on-the-fly. Several test cases are conducted to investigate the effects of mesh resolution on the DDT process in the smooth detonation chamber. The radius of the initial high temperature region is elevated to 10mm and its pressure is 1MPa to shorten the DDT distance in the test cases. The grid independence on the DDT parameters is demonstrated in Table 2. As Table 2 indicates, the DDT occurs at an inaccurate position in the three-level refinement case owing to the lower grid resolution. By contrast, the four-level refinement is enough to capture the correct location where the flame transforms to detonation. Although the DDT time is prolonged about eight percent compared to the five-level refinement case, the four-level refinement is considered as a converged mesh resolution in these DDT simulations, which balances the simulation resolution and computing effectiveness for engineering applied simulations.

In this paper, computations were conducted on the Tianhe-2 Supercomputer center platform, where 120 cores of Intel Xeon E5-2692V2 (2.2 GHz) were used for each run. Typical runtimes for the DDT process are proximately 48h.

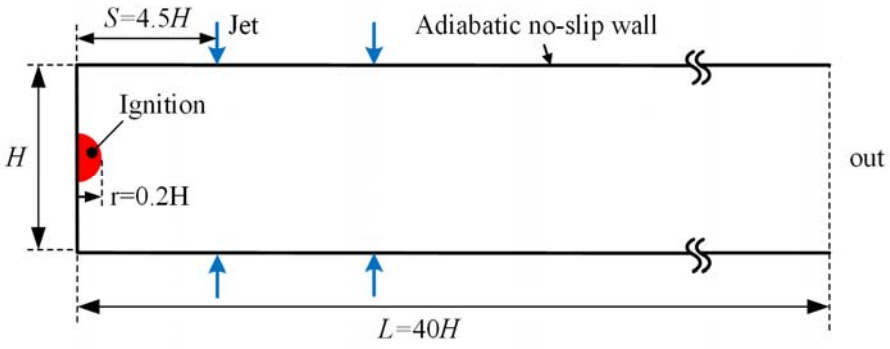

Fig. 4. Schematic diagram of the computational domain

Table 2. Mesh refinement study

Refinement levels	Refinement mesh size (mm)	DDT distance (mm)	DDT time (ms)	Total runtimes (cpu·h)
3	0.125	149.070	0.369	224
4	0.0625	269.635	0.617	3686
5	0.03125	267.428	0.566	9699

3. Results and discussions

3.1 Experimental results

3.1.1 The effect of a single jet on flame acceleration and propagation

The influence of a single JICF on the flame acceleration process with different injection location were investigated firstly. Figure 5 shows the time sequence of high-speed photographing images. The evolution of the flame in a smooth tube is depicted in Figure 5(a). It is revealed that the entire flame propagation process of the case without jet flame can be divided into four distinct phases: the initial flame core, the flame with bifurcated front, the finger flame and the fast deflagration flame. Firstly, the spark plug forms the initial flame, then the flame propagates to the right. It is noted that the initial laminar flame core quickly transforms into a turbulent flame resulting in the flame bush at the front. At the second stage, the flame front macroscopically splits into two independent flame cusps, spreading near the upper and lower wall, respectively. At the next stage, the flame accelerates continuously and the bifurcated surface is merging gradually (Fig.5 (a) t=1.875ms). The flame front develops to a finger shape. Ultimately, the flame continues to accelerate and exhausts into the atmosphere by breaking through the thin film at the right end. The finger flame can be accelerated to a fast deflagration with a velocity of 1558m/s. The flame front becomes brighter compared with the previous stages.

The effect of a single jet located at x=90mm on the flame propagation is demonstrated in Figure 5 (b). Although depiction of the interaction between the jet and flame is limited by the camera resolution, there is a distinct change that the bifurcated flame surface merges in advance compared with Case 1. The flame finally accelerates to the exit with high velocity but there is no detonation observed.

Figure 5 (c) shows the evolution of the flame in Case 3, the jet being located at x=180 mm. Similar to Case 2, the flame in Case 3 spreads faster than that in the smooth case because of the earlier coalescent flame front. Subsequently, the flame gradually accelerates, forming a fingertip flame at t=1.458ms. Unlike the previous cases, the flame runs up to a detonation, which leads to the flame utter brightness (Figure 5 (c) t=1.666ms). The overdriven detonation abruptly releases enormous energy with bright light. As a result, it seems like the channel broadened visually at the transition position.

The jet location determines the flow structure of unburned gas when the flame hits the jet. In Case 2, the jet spays into the flow field closing the initial flame core. The velocity is relatively high compared with the mainstream, which means that the

jet leads to blockage at an early stage. On one hand, this effect is detrimental for the flame propagation. On the other hand, the jet stream strengthens the local turbulence intensity and enhances flame acceleration. However, the effect of blockage is dominant when the velocity of the mainstream is low. In Case 3, the jet injection from x=180mm has a negligible effect on the initial flame core, but the flow perturbation is conducive for flame spread, and the flame velocity subsequently jumps.

It is revealed that the jet location is a significant parameter because different flame structures are formed in different positions of the channel. As a consequence, the effect of the jet on the flame acceleration is different.

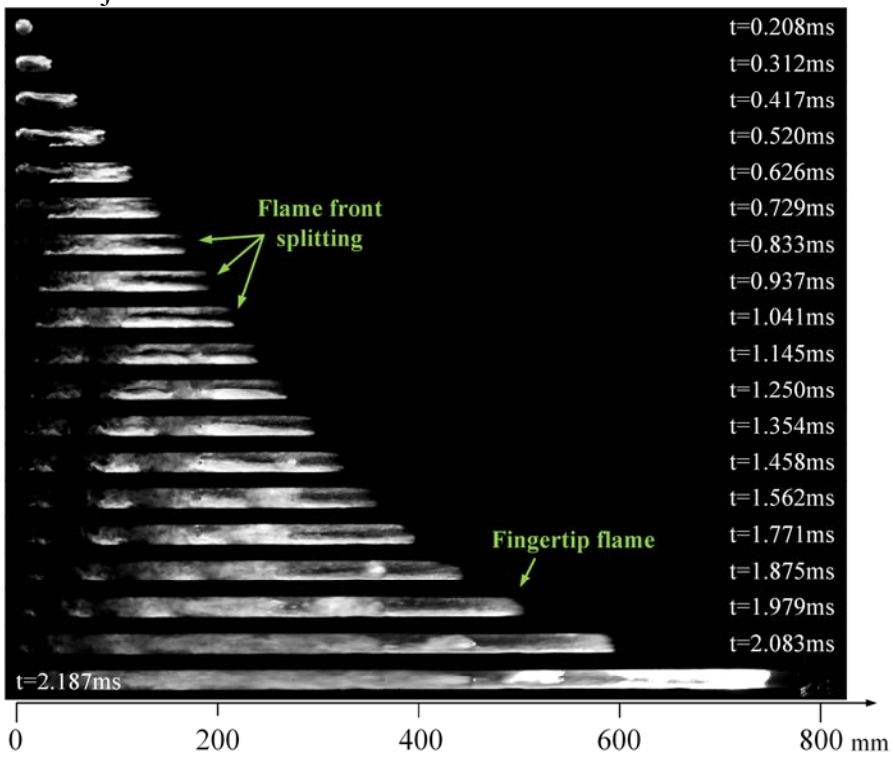

(a) case1

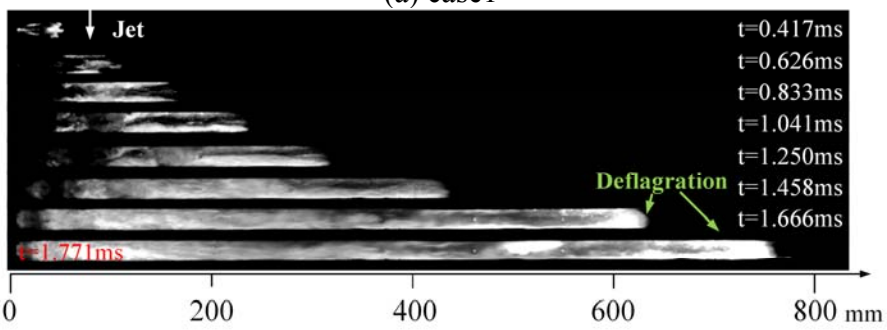

(b) case2

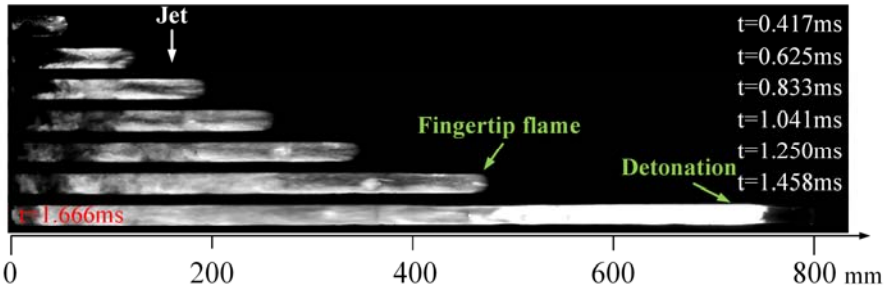

(c) case3

Fig. 5. Flame propagation in the tube visualized by high-speed photography

Figure 6 shows the flame speed over time for the three conditions above. The theoretical CJ detonation velocity of stoichiometric methane/oxygen under corresponding initial condition is calculated by the Chemkin chemical equilibrium module, which is denoted by the dashed line in Fig. 6. The typical DDT phenomena obtained by the experiments includes three stages. At the first stage, the initial flame gradually accelerates to a fast-propagating flame with about half C-J velocity. At the second stage, the fast-propagating flame abruptly accelerates to a high speed (mostly above C-J velocity) and transitions to an overdriven detonation wave, which is also the criterion for DDT time and distance in this study. At the last stage, the detonation decays and propagates to the exit. The flame propagation speed peak of the smooth tube case is 1558 m/s, about 65.8% of the CJ value, which means that under this condition the flame cannot accelerate to a detonation within the effective shooting length. The velocity of flame propagation in cases with jet injection is obviously accelerated. The case with jet located at 90mm does not accomplish the detonation transition as well, but the flame is accelerated faster and propagates to the exit, taking less time compared with the smooth channel case. The case with jet position 180mm generates a bright overdriven detonation before the exit as shown in Fig.5(c), and the velocity of this case reaches 110% of the theoretical CJ value.

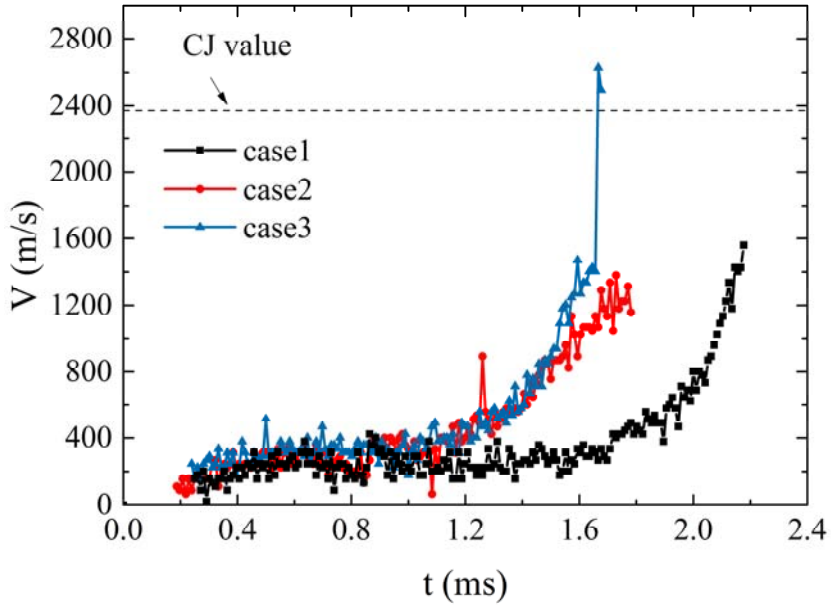

Fig. 6. Diagram of flame propagation velocity versus time in experiments

3.1.2 The effect of jet arrangements on the flame acceleration

Figure 7 shows the effect of the two jets varying arrangements on flame spread over time. The single jet in Case 2 can only reach the flame speed of about one half CJ theoretical value, which cannot produce a detonation within the length of the tube, but the double jets have a greater influence on the DDT process. Compared with the single jet, double jets can produce more turbulence in the manifold, which can facilitate the propagation of a turbulent flame at early stage. As a result, the transition of deflagration to detonation is completed earlier.

In these cases, the flame spreads faster from the initial stage; the flame speed with double jets disturbance is greater than that with the single jet disturbance. Comparing the Figs. 5 and 7, it is apparent that the combustion intensity is enhanced with brighter fluorescence. The flame in the double jets cases propagates faster, and rapidly transforms from deflagration to detonation. Although direct observation of jet and flame interaction is ambiguous due to the limited spatial resolution, the transition point is distinct. The various jet arrangements lead to disparate DDT distances.

It is interesting to note that the effect of the impinging jet is sensitive to the jet location. When the jets are positioned at the forepart (x=90mm), the flow blockage hinders the initial flame propagation. However, when the jets are located at the relatively rear position (x=180mm), the blocking effect of the jets is marginal and the reinforcement of turbulence intensity plays a dominant role on flame acceleration.

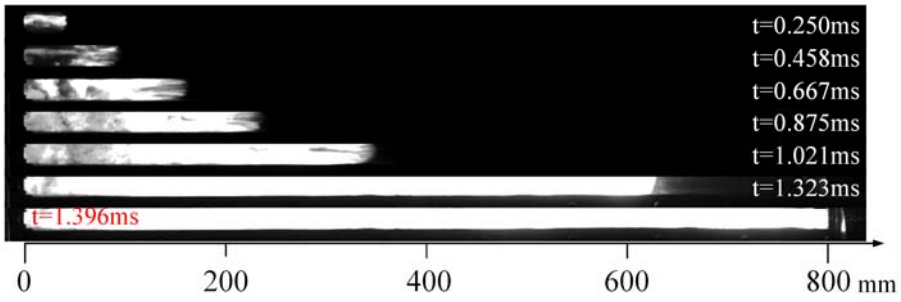

(a) case4

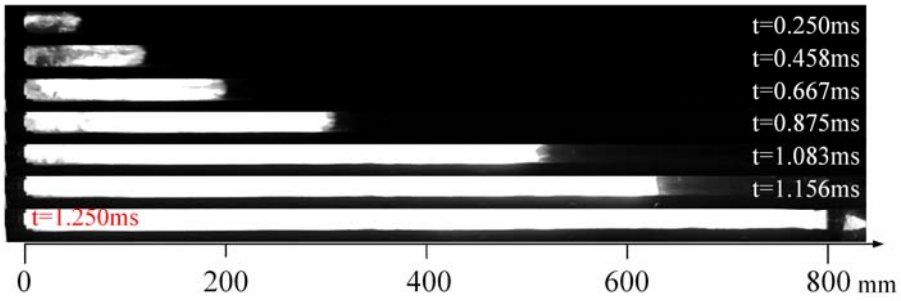

(b)case5

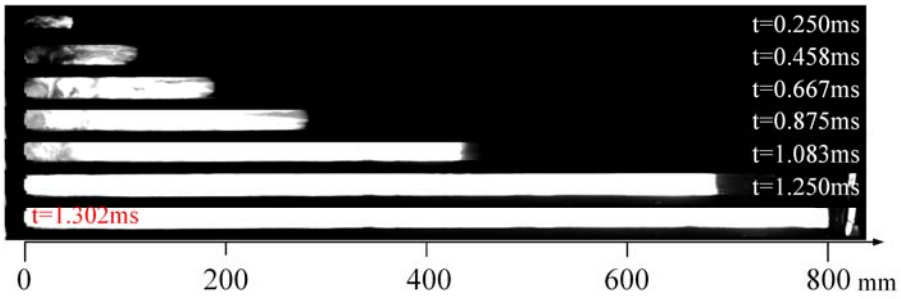

(c) case6

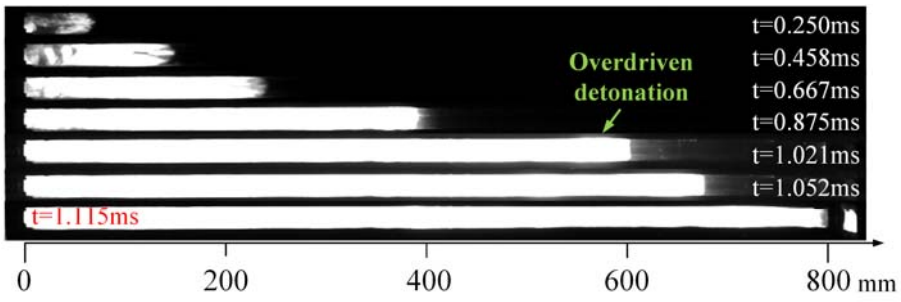

(d) case7

Fig. 7. Flame propagation in the tube visualized by high-speed photography for two jets in different arrangements (see Table 1)

The different forms of double jets are demonstrated to obtain a shorter DDT time compared with a single jet. The corresponding flame speed curves are shown in Fig. 8. As the mixture is ignited, the initial flame kernel expands slowly. The presence of the jets leads to the formation of vortices ahead of the flame front. The flame is distorted by the jet entrainment when it passes through the vortices' inner region. The flame structure is evolving and it becomes very bright in the middle of the manifold, then develops into the detonation wave.

The shortest time of DDT is about 1.01 ms, when the jet type is that of staggered jets. A 60% decrease in the DDT distance and a 39% decrease in the DDT time are observed for this case comparing to a single JICF (Case 3). The two jets are injected reversely, and the resulting vortices are oriented in the same direction. Vorticity greatly increases the burning rate, and then the flame rearing the precursor shock accelerates to a detonation wave. In Case 5 and 7, although the flame quickly accelerated to a high velocity (over the C-J velocity) and transitioned to an overdriven detonation, it decays rapidly to a deflagration with a velocity of 1458 m/s and 1348 m/s, respectively.

Various degrees of detonation decay are observed in the experiment. A preliminary explanation is that there is not enough combustible mixture to sustain the detonation propagation to the end of the tube because the thin film is broken up ahead of time when the detonation arrived. The combustible mixture near the exit is therefore diluted by atmospheric air.

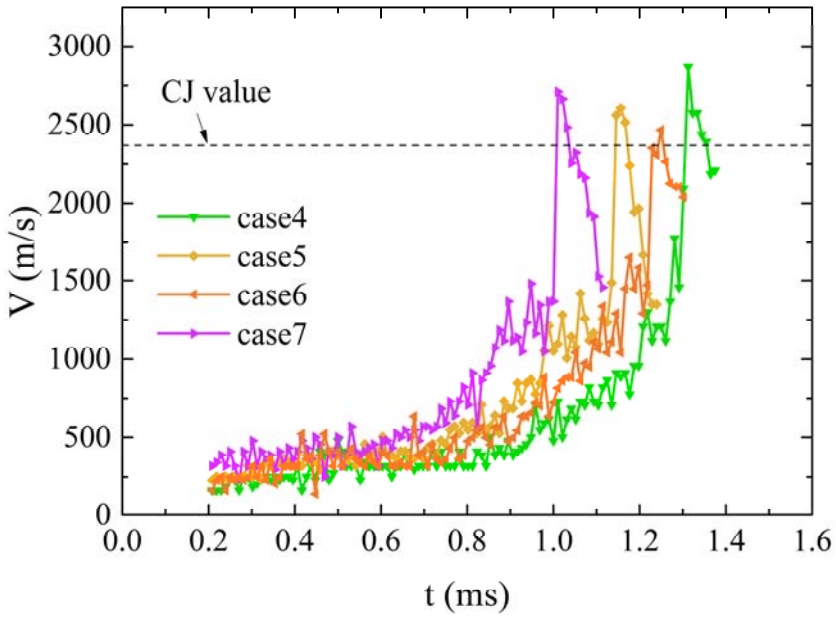

Fig. 8. Diagram of flame propagation velocity versus time in experiments

The main uncertainty of the experiment is caused by the accuracy of the jet control. The relay and solenoid valves both have uncertain response times, which has an influence on the relatively short flame propagation period. The jet injection start determines the exact jet injection duration and this influences the flame propagation progress and the structure of unburned gas in front of the flame. Note that there are slight variations in the jet injection start moment despite an identical delay time setting.

3.2 Numerical simulations results

Figure 9 shows the flame speed variation history of all the cases. For the smooth tube, Case 1, the flame initially experiences an acceleration process, and then the flame velocity reaches about 400m/s on average. The flame eventually propagates to the right outlet but has failed to produce the detonation. As shown in this figure, the majority of cases with JICF completed the transition to the detonation before the exit, except for the case with single jet located at x=180mm. The flame of each case with eventual detonation gradually accelerates and achieves a high velocity (over the C-J velocity), resulting in the completed transition into an overdriven detonation, which soon experiences deficits and oscillates within five percent above the CJ speed value. In general, the double jets can dramatically increase the occurrence rate of detonation compared with the single jet and the smooth tube case.

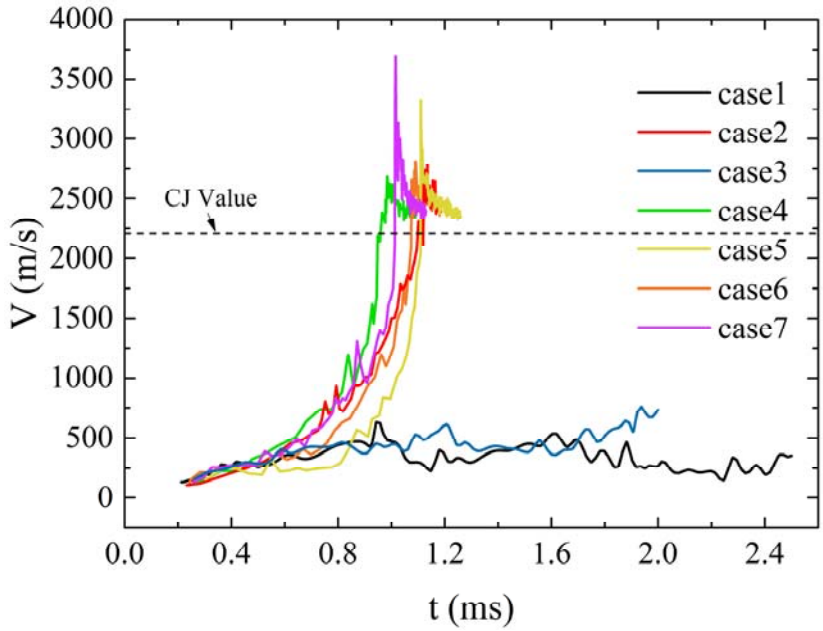

Fig. 9. Diagram of flame propagation velocity versus time in the numerical simulations

Figure 10 shows the temperature contours diagram of various cases at the time of transition to detonation. The DDT distance in Case 5 is the shortest. Although the flame undergoes a relatively long acceleration process, it finally triggers the local explosion on the upper and lower walls of the pipe at x=420.1 mm. This figure also depicts that there are some differences among the various jet arrangements, and in addition, the double jets can clearly shorten the DDT distance compared with the single jet Case 2.

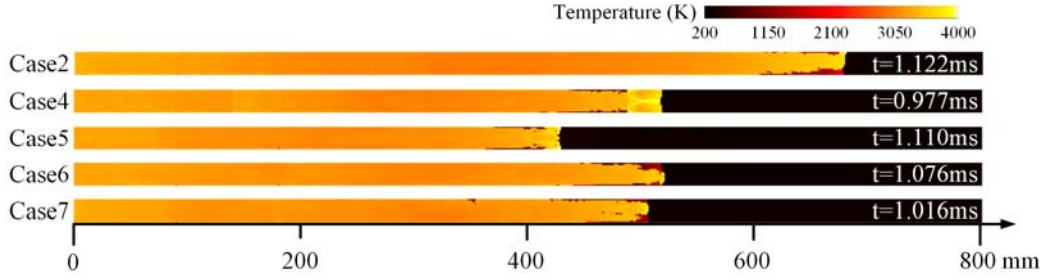

Fig. 10. Temperature contours of various cases at the time at which the local explosion is occurring

In order to have a better understanding of the influence of JICF on the flame acceleration and DDT process, Case 2 with single jet is firstly analyzed in detail. Figure 11 (a) gives a flame temperature contours time sequence of Case 2. Firstly, the initial semicircle flame core expands radially, but soon it is influenced by the pressure wave reflected off the wall. As shown, the flame front wrinkles and gradually spreads towards the open right end. The jet impacts the mainstream and induces large-scale vorticities. When the flame goes through these vorticities, the flame front surface is distorted and wrinkled (Fig.11(a) t= 0.793ms, t=0.844 ms). The accelerated flame gradually approaches the leading shock wave and suddenly transforms into a local explosion (Fig.11(a) t = 1.122 ms). The local explosion develops to a global overdriven detonation (Fig.11(a) t= 1.130 ms), then promptly decays to the stable detonation propagation.

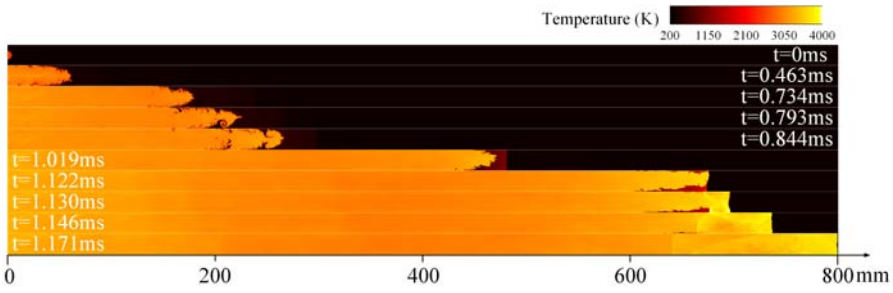
Temperature (K)
200 1150 2100 3050 4000
t=0ms
t=0.463ms
t=0.734ms
t=0.793ms
t=0.844ms
t=1.019ms
t=1.122ms
t=1.130ms
t=1.146ms
t=1.171ms
0
200
400
600
800mm

a)

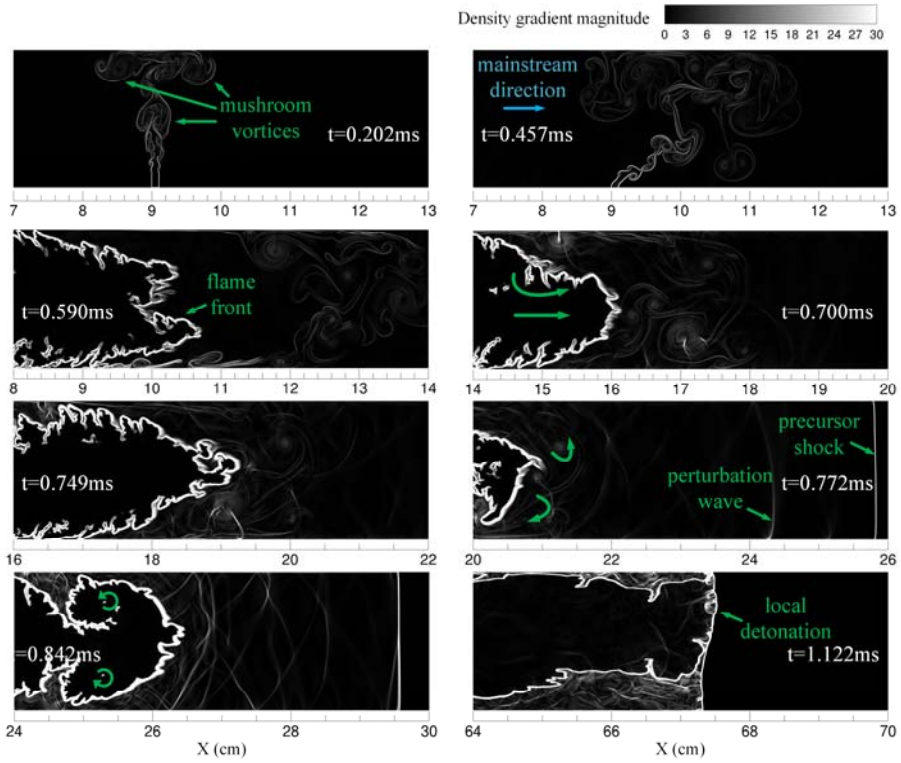
Density gradient magnitude
0 3 6 9 12 15 18 21 24 27 30
mushroom
vortices
t=0.202ms
mainstream
direction
t=0.457ms
flame
front
t=0.590ms
t=0.700ms
t=0.749ms
precursor
shock
perturbation
wave
t=0.772ms
local
detonation
t=1.122ms
X (cm)
X (cm)

b)

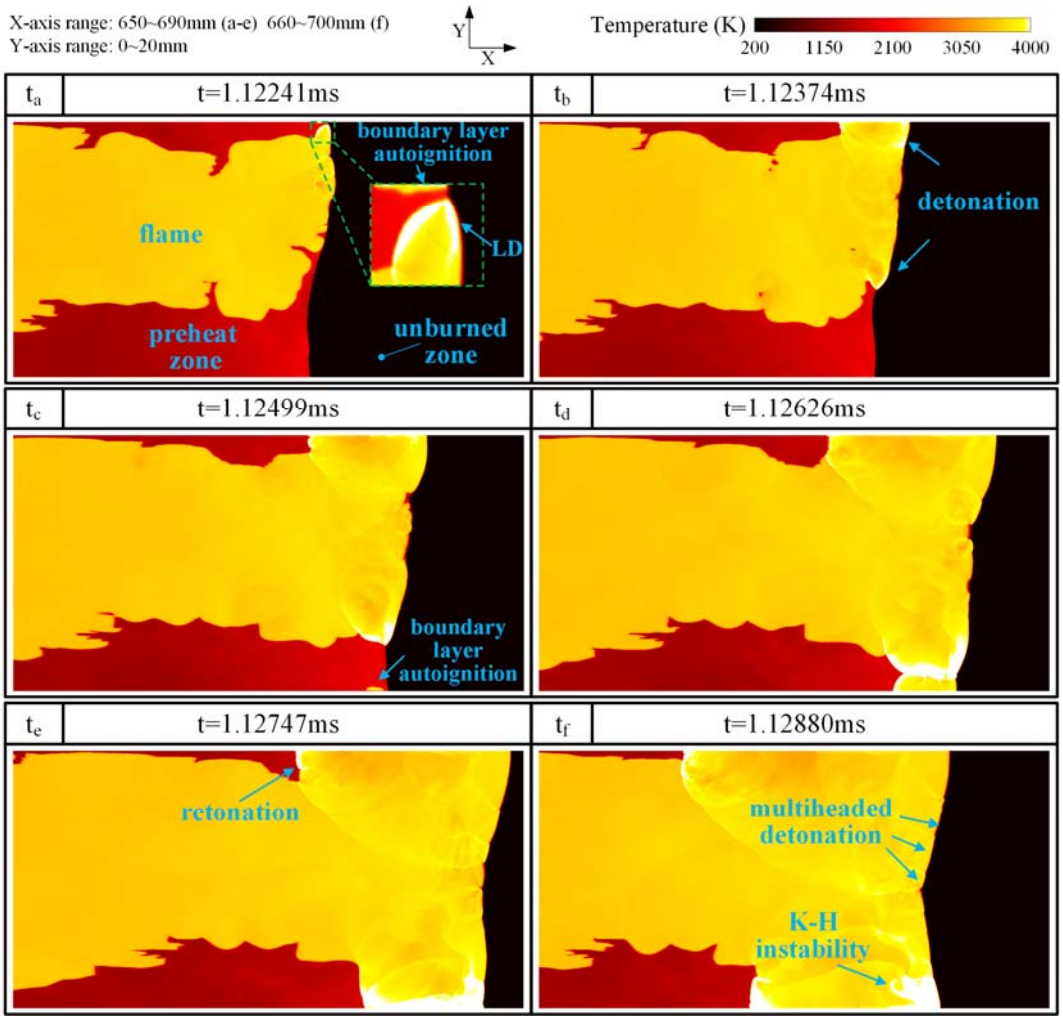

(c)

Fig. 11 Sequence diagram of the interaction of flame and jet of case2, a) temperature contours, b) density gradient magnitude contours and c) the locally zoomed segments of (a) at the transition instant (L-D: local detonation)

Figure 11 (b) shows the density gradient magnitude change of the local flow field in Case 2. The jet enters from the bottom wall. After a temporary unperturbed propagation, it impacts on the top wall and forms the rotating coherent structures, named mushroom vortices [29]. The mushroom structure is composed of a pair of counter-rotating vortices; the right side of it rotates clockwise, while the left side rotates counterclockwise. The leading mushroom vortices spread along up- and downstream, respectively. The follow-up trailing vortex caused by Kelvin-Helmholtz instability vertically rises and joins into the leading mushroom vortices. Then, influenced by the mainstream, the jet is gradually deflected in the downstream direction. The subsequent spiral vortices no longer enter the mushroom vortices. Some small vortices start merging and interacting with each other randomly. This indicates that the penetration ability of jet is rapidly decreased.

When the flame front approaches the jet exit, the fresh jet is extruded to abutting the lower wall (Fig.11(b) t= 0.590 ms). The bifurcate flame front starts merging due to the counterclockwise vorticity effect (Fig.11(b) t= 0.700 ms). Then the flame is curved and stretched by the vorticity, and the surface area is increased quickly.

Further, the local enhanced diffusion leads to the heat release rate rising. As a result, the flame speed is rapidly elevated.

Moreover, the interaction between flame and JICF vorticity produces weak perturbation waves (Fig.11(b) t=0.842ms), which strengthens the intensity of the precursor shock. Finally, the accelerated flame front catches up with the leading shock wave, and triggers the localized detonation (Fig.11(b) t=1.122ms).

In addition, the local detailed temperature contours at the transition moment are given in Fig. 11(c). On the one hand, the flame is gradually accelerated and the local detonation is triggered at the existing flame front by the coupling of the flame and the precursor shock. On the other hand, the leading shock wave compresses the unburned material and the hot spots occur in the boundary layer. Then the local detonation interacts with boundary layer autoignition, collides with the wall and is enhanced. The detonation subsequently expands to the whole cross section. A retonation wave is observed in the process, because of the unburned material between the leading shock wave and the wrinkled flame front.

Figure 12 reveals the impinging jet evolution in the channel of Case 4. The process can be characterized by three stages. At the first stage, the JICFs form the mushroom vortices respectively in the vertical direction. When the jet impinges, the vortices are separated and restructured into two new leading mushroom vortices propagating along the axial direction up and down stream (Fig. 12 t=0.152ms). At the second stage, due to the effect caused by the mainstream flow, the fresh jet inclines downstream. Compared with the mushroom structure derived by the single jet hitting the wall in Case 2, the vortices in this case are larger and spread upstream further, which leads to an early interaction with the flame front (Fig. 12 t = 0.498). At the last stage, conspicuous distortion is observed in the flame front surface owing to the downstream leading mushroom vortices, and the flame is abruptly accelerated again. In this case, a 14% decrease in the DDT distance and a 27% decrease in the DDT time are observed comparing to a single JICF (Case 2).

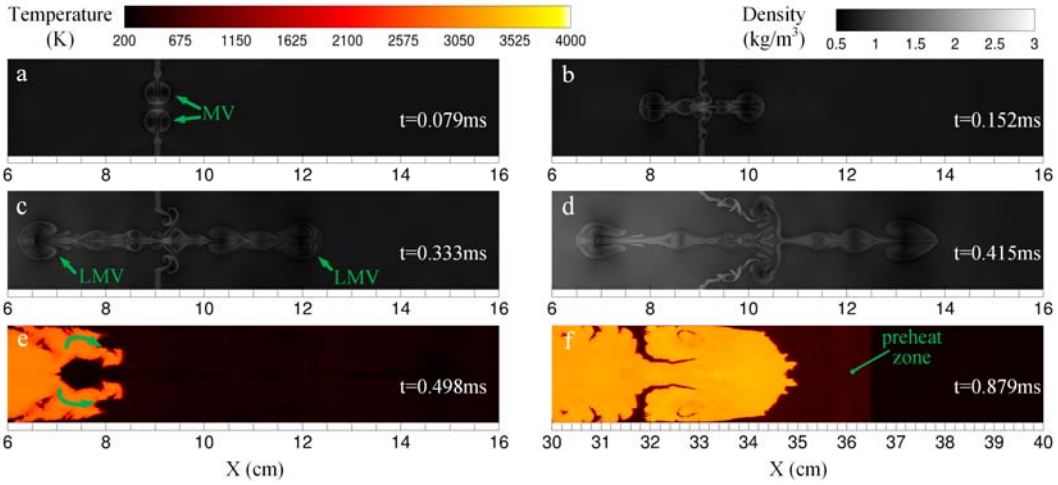

Fig. 12 Sequence diagram of the interaction of flame and jet of case4, density contours (a, b, c, d) and temperature contours (e, f) (MV: mushroom vortices; LMV: leading mushroom vortices)

Figure 13 shows the sequence diagram of flame propagation influenced by parallel jets. In this Case, the evolution process of the separate jet is similar to that in Case 2, and there is no obvious interaction between the twin jet stream at early stage (Fig. 13 t=0.244ms). When the flame front touches the leading mushroom vortices, it is influenced by the left side counterclockwise vorticity (Fig. 13 t=0.601ms). The lee-

side mushroom vortices spread downstream, but it is affected by the rear mushroom vortices induced by the jet at x=180mm. Hence, the front mushroom vortices have to move toward the bottom, then the mushroom vortices are gradually weakened after colliding with the wall (Fig. 13 t=0.717ms). After that, the flame continues to spread downstream and is accelerated under the influence of the rear vortices induced by the jet stream.

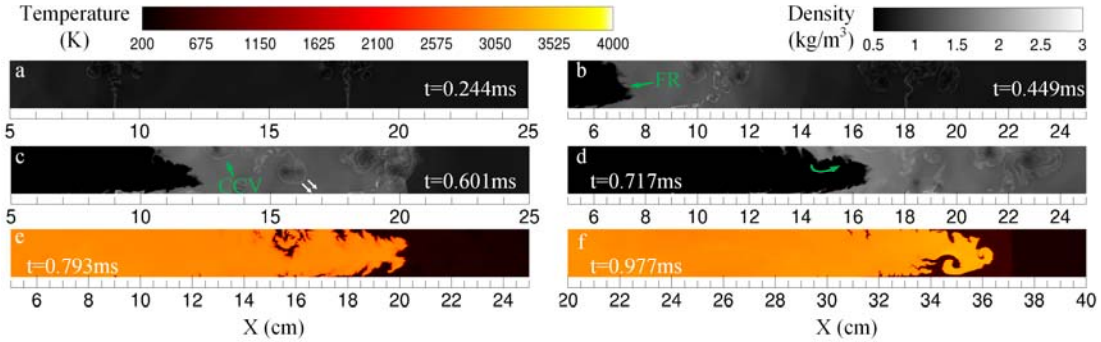

Fig. 13 Sequence diagram of the interaction of flame and jet of case6, density contours (a, b, c, d) and temperature contours (e, f) (FR: flame front; CCV: counterclockwise vorticity)

Figure 14 indicates the interactions between the flame and vortices in Case 7. The left side counterclockwise vorticity in the leading mushroom leads the tendrils of the flame, and the right side clockwise vorticity developed downstream. Compared with Case 6, the rear mushroom vorticities influence the leading mushroom clockwise vorticity less. Subsequently, the flame is curved by the leading right side clockwise vorticity (Fig.14 t=0.833ms). This extra acceleration explains the phenomenon that staggered jets appreciably shorten the DDT distance and time in comparison to parallel jets. Finally, the rear mushroom structure evolves into a large-scale clockwise vorticity, which warps the flame front surface and enhances the combustion (Fig.14 t=0.918ms).

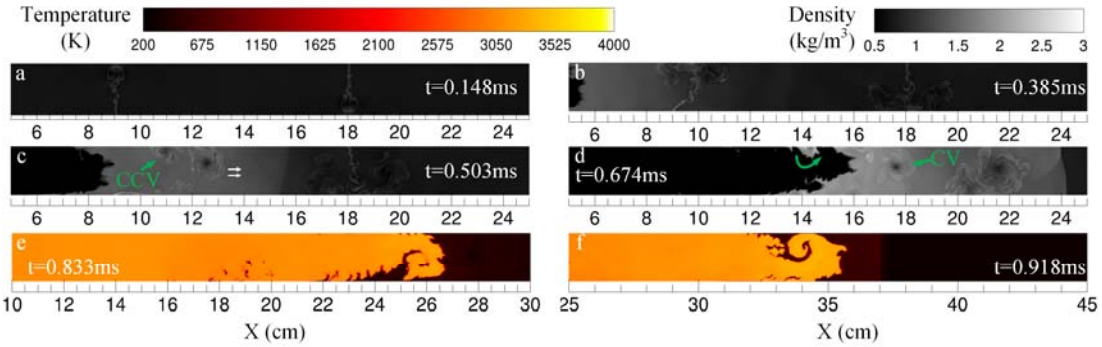

Fig. 14 Sequence diagram of the interaction of flame and jet of case7, density contours (a, b, c, d) and temperature contours (e, f) (CCV: counterclockwise vorticity CV: clockwise vorticity)

The results of experiment and numerical simulation both reveal that the JICF can distinctly shorten DDT time and distance. However, it is noted that there are some differences between the two methods. First of all, although the methane oxygen premix gas is stoichiometric in both methods, the numerical simulation case is diluted by 25% of the volume fraction nitrogen. Secondly, in the experiment, the jet exit is a circular hole, which inevitably has a three-dimensional effect. On the other hand, in the two-dimensional numerical simulation, the jet exit corresponds to a slot that would have infinite length in the third dimension. Its influence on the mean flow will therefore naturally be enhanced in the strictly two-dimensional case. Moreover, due to

the uncontrollability and randomness of the DDT process, it is difficult to completely reproduce DDT experimental results by numerical simulation.

The essential differences between the experimental and numerical simulation results are the following: In the experiments, jets located at 180mm have a better effect on flame acceleration than jets injected from 90mm. This is opposite to the numerical simulation results. A preliminary analysis is that the actual ignition model and mixture inhomogeneity lead to a low mainstream flame propagation speed at early stage, which means that the jet penetration ability is stronger. Hence, when the jet position changes, resulting flow field disturbances change correspondingly, which further impacts on flame acceleration. In addition, in the cases failing to transition into a detonation, the flame in the experiment can accelerate to about half CJ velocity, while the flame velocity in the numerical simulations reaches only a quarter of the CJ value on average. This can be explained by the fact that the membrane is set as the right exit boundary for the experiment, which plays the role of a solid wall at the initial stage. Incipient weak pressure waves can be reflected at the right wall, then spread back to accelerate the flame.

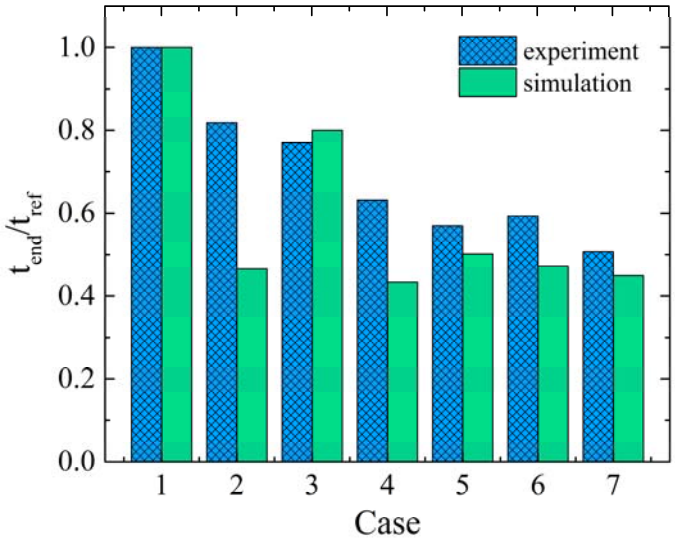

Fig. 15 flame propagation normalized time between experiment and numerical simulation

As figure 15 shows, the normalized time is a good indicator to compare experiment and numerical simulation. The normalized time is identified as the flame propagation time for arriving at the exit in this case divided by that in Case 1. It is indicated that the reactive JICF can accelerate the flame speed and shorten the flame propagation time. Moreover, there still are some qualitative similarities between experiment and numerical simulation results. For example, the probability of detonation occurrence can be significantly improved by the jet stream, and the effect of double jets on flame acceleration is better than that of a single jet. Further, the staggered jets perform better than parallel jets on the DDT process.

4. Conclusions

A series of experiments and related two-dimensional numerical simulations have been conducted in the present work to investigate the effect of reactive JICF on flame acceleration and DDT process. Various jet arrangements within the detonation tube, including single jet, impinging jets, double parallel jets and staggered jets, have been

investigated to quantify their influence on a single cycle detonation experiment. Furthermore, the evolution of jet stream structure, the interaction between the jet and flame are characterized by the corresponding numerical simulations. The results show that the probability of detonation occurrence can be improved by the JICF and the JICF can shorten the DDT distance and time in the detonation chamber. The double jets perform better than a single jet in accelerating the flame. In the experiments, the staggered jets provide optimal flame acceleration. A 60% decrease in the DDT distance and a 39% decrease in the DDT time are observed for this case compared to a single JICF. In the numerical simulations, the impinging jets (located at x=90mm) performs better with a 14% decrease in the DDT distance and a 27% decrease in the DDT time by comparison with a single JICF.

The simulations confirm that the jet induced mushroom vorticities, composed by counter-rotating vortex pairs, are undisputedly playing a significant role in the DDT process. The flame is distorted and curled through the vortex region, which expands the flame front surface rapidly, and consequently leads to the diffusion enhancement and heat release rate rise. Therefore, the effect on the flame acceleration from the jet is influenced by the vortex structure when the flame interacts with the jet, which means that the various jet axial locations and injection types will make a clear difference on flame propagating evolution and acceleration. The impinging jets create a relatively highspeed upstream vortex, which is ahead of the flame-vortex interaction, but meanwhile causes more blockage. The staggered jets perform better than parallel jets in both experiment and simulation because of the reduced influence between the two mushroom structures induced by different jet locations. However, it still needs more experiments and numerical simulations to explore the appropriate jet parameters including injection angle, jet pressure and temperature in the future work for jet turbulator design of pulsed-detonation engines.

Acknowledgments

This research is sponsored by the National Natural Science Foundation of China (Grant No. 51406171 and 91441128), Fundamental Research Funds for the Central Universities of China (Grant No. 20720180058), Aeronautics Power Foundation (Grant No. 6141B090325) and the Natural Science Foundation of Fujian Province (Grant No. 2015J05111).

References

[1] Y.H. Wu, F.H. Ma, V. Yang, System performance and thermodynamic cycle analysis of airbreathing pulse detonation engines, J. Propul. Power 19 (2003) 556-567.

[2] W.H. Heiser, D.T. Pratt, Thermodynamic cycle analysis of pulse detonation engines, J. Propul. Power 18 (2002) 68-76.

[3] M. Cooper, S. Jackson, J. Austin, E. Wintenberger, J.E. Shepherd, Direct experimental impulse measurements for detonations and deflagrations, J. Propul. Power 18 (2002) 1033-1041.

[4] W. Fan, C.J. Yan, X.Q. Huang, Q. Zhang, L.X. Zheng, Experimental investigation on two-phase pulse detonation engine, Combust. Flame 133 (2003) 441-450.

[5] S.Y. Lee, J. Watts, S. Saretto, S. Pal, C. Conrad, R. Woodward, R. Santoro, Deflagration to detonation transition processes by turbulence-generating obstacles in pulse detonation engines, J. Propul. Power 20 (2004) 1026-1036.

[6] G. Ciccarelli, S. Dorofeev, Flame acceleration and transition to detonation in ducts, Prog. Energy Combust. Sci. 34 (2008) 499-550.

[7] S. Emami, K. Mazaheri, A. Shamooni, Y. Mahmoudi, LES of flame acceleration and DDT in hydrogen-air mixture using artificially thickened flame approach and detailed chemical kinetics, Int. J. Hydrogen Energy 40 (2015) 7395-7408.

[8] V.N. Gainezo, T. Ogawa, E.S. Oran, Numerical simulations of flame propagation and DDT in obstructed channels filled with hydrogen-air mixture, Proc. Combust. Inst. 31 (2007) 2463-2471.

[9] C.M. Brophy, W.T. Dvorak, D.F. Dausen, C.B. Myers, Detonation initiation improvements using swept-ramp obstacles, 48th AIAA Aerospace Sciences Meeting Including the New Horizons Forum and Aerospace Exposition (2010), paper 1336.

[10] K.A. Ahmed, D.J. Forliti, Fluidic Flame Stabilization in a Planar Combustor Using a Transverse Slot Jet, Aiaa J. 47 (2009) 2770-2775.

[11] B.W. Knox, D.J. Forliti, C.A. Stevens, J.L. Hoke, F.R. Schauer, Unsteady flame speed control and deflagration-to-detonation transition enhancement using fluidic obstacles, 48th AIAA Aerospace Sciences Meeting Including the New Horizons Forum and Aerospace Exposition (2010), paper 151.

[12] B.W. Knox, D.J. Forliti, C.A. Stevens, J.L. Hoke, F.R. Schauer, A comparison of fluidic and physical obstacles for deflagration-to-detonation transition, 49th AIAA Aerospace Sciences Meeting Including the New Horizons Forum and Aerospace Exposition (2011), paper 587.

[13] S. Zhao, Y. Fan, H. Lv, B. Jia, Effects of a jet turbulator upon flame acceleration in a detonation tube, Appl. Therm. Eng. 115 (2017) 33-40.

[14] J.P. McGarry, K.A. Ahmed, Laminar deflagrated flame interaction with a fluidic jet flow for deflagration-to-detonation flame acceleration, 51st AIAA/SAE/ASEE Joint Propulsion Conference (2015), paper 4096.

[15] J. Chambers, K.A. Ahmed, Turbulent flame augmentation using a fluidic jet for Deflagration-to-Detonation, Fuel 199 (2017) 616-626.

[16] J.P. McGarry, K.A. Ahmed, Flame-turbulence interaction of laminar premixed deflagrated flames, Combust. Flame 176 (2017) 439-450.

[17] E.S. Oran, V.N. Gamezo, Origins of the deflagration-to-detonation transition in gas-phase combustion, Combust. Flame 148 (2007) 4-47.

[18] D.A. Kessler, V.N. Gamezo, E.S. Oran, Simulations of flame acceleration and deflagration-to-detonation transitions in methane-air systems, Combust. Flame 157 (2010) 2063-2077.

[19] V.N. Gamezo, T. Ogawa, E.S. Oran, Flame acceleration and DDT in channels with obstacles: Effect of obstacle spacing, Combust. Flame 155 (2008) 302-315.

[20] C.J. Wang, J.X. Wen, Numerical simulation of flame acceleration and deflagration-to-detonation transition in hydrogen-air mixtures with concentration gradients, Int. J. Hydrogen Energy 42 (2017) 7657-7663.

[21] C. Johansen, G. Ciccarelli, Numerical simulations of the flow field ahead of an accelerating flame in an obstructed channel, Combust. Theor. Model 14 (2010) 235-255.
[22] R. Deiterding, Parallel adaptive simulation of multi-dimensional detonation structures Ph.D. Thesis, Brandenburgische Technische Universität Cottbus, Cottbus, 2003.
[23] R. Deiterding, A parallel adaptive method for simulating shock-induced combustion with detailed chemical kinetics in complex domains, Comput. Struct. 87 (2009) 769-783.
[24] J.L. Ziegler, R. Deiterding, J.E. Shepherd, D.I. Pullin, An adaptive high-order hybrid scheme for compressive, viscous flows with detailed chemistry, J. Comput. Phys. 230 (2011) 7598-7630.
[25] R. Deiterding, S. Wood, Parallel adaptive fluid-structure interaction simulation of explosions impacting on building structures, Comput. Fluids 88 (2013) 719-729.
[26] X.D. Cai, J.H. Liang, R. Deiterding, Y. Mahmoudi, M.B. Sun, Experimental and numerical investigations on propagating modes of detonations: Detonation wave/boundary layer interaction Combust. Flame 190 (2018) 201-215.
[27] G. Dong, H.W Liu, Y.L. Chen, General, nitrogen-containing semi-detailed chemical kinetic mechanism for methane laminar premixed flame, J. Combust. Sci. Technol. 8 (2002) 44-48.
[28] G. Dong, B.C. Fan, B. Xie, J.F. Ye, Experimental investigation and numerical validation of explosion suppression by inert particles in large-scale duct, Proc. Combust. Inst. 30 (2005) 2361-2368.
[29] R.F. Huang, J. Lan, Characteristic modes and evolution processes of shear-layer vortices in an elevated transverse jet, Phys. Fluids 17 (2005) 034103.